

Nanoindentation, Scratch, and Elevated Temperature Testing of Cellulose and PMMA Films

Application Note

Introduction

As plastics and plastic composites are placed into service in more demanding applications, surface modifications are performed to enhance the durability and increase service life. Commonly, hard coatings are used on display screens to prevent damage; for example, coatings are applied to cellular telephone display screens to prevent scratching while the phone is placed in a pocket with keys and other sharp objects. Other surface modifications are made to increase adhesion of multilayered systems, create fade resistant properties, or to increase flexibility. In this article, polymer films with different surface treatments are characterized through nanoindentation, scratch testing,

and elevated temperature testing. Major differences in the indentation and scratch results are shown for the coated samples. In addition, the results for elastic modulus and hardness at elevated temperatures are supplied on four different cellulose films.

Samples

Seven polymer samples were supplied by a display screen manufacture. The samples were triacetyl cellulose film (coated and uncoated), coated poly(methylmethacrylate) (PMMA), acetate propionate cellulose films, and alcohol saponification cellulose. Table 1 lists each sample and supplies a description.



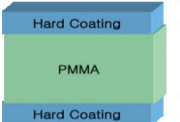
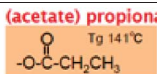
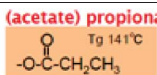
Sample	Description	Sample Geometry
A	triacetyl cellulose film (TAC)	 80µm Triacetyl Cellulose Film
B	Coated TAC	 13µm UV Cured Hard Coating Film 80µm Triacetyl Cellulose Film
C	Coated PMMA	 10µm UV Cured Hard Coating 800µm Polymethylmethacrylate Sheet 10µm UV Cured Hard Coating
D-1-1 (before)	acetate propionate cellulose	 (acetate) propionate T _g 141°C <chem>CC(=O)OCC1OC1</chem>
D-1-2 (after)	Alcohol saponification cellulose	
D-2-1 (before)	acetate propionate cellulose	 (acetate) propionate T _g 141°C <chem>CC(=O)OCC1OC1</chem>
D-2-2 (after)	Alcohol saponification cellulose	

Table 1. Sample descriptions.

Test Equipment

All of the tests conducted in this article were performed using an Agilent Nano Indenter G200 equipped with the XP transducer that combines superb load and displacement resolutions with unmatched flexibility in force and displacement ranges. The XP transducer is a Nanomechanical Actuating Transducer (NMAT) that is used to apply loads and measure displacements during indentation tests. Its novel design includes decoupled force application and displacement measurement for unparalleled control and flexibility during testing. A cross-section of the XP-NMAT is shown in Figure 1.

Each of the design elements shown in Figure 1 contribute to the repeatable and reliable measurements performed by the Nano Indenter systems. Control of force is performed using electromagnetic actuation providing three primary advantages:

- 1) High accuracy in force control due to the simple linear relationship between current passed through the coil and the force that is produced.
- 2) Force application over a large displacement range due to the stability of the permanent magnetic field over large distances.
- 3) Flexible force application in both actuating directions because electromagnetic actuation works equally well in both the push and pull directions.

Two leaf springs are used to secure the indentation column for stability and maximum lateral stiffness. The ISO 14577 standard specifies that the samples surface should be within one degree of orthogonal alignment with the indenter; in actuality, this is not just a recommendation, it is a must for repeatable and reliable data. As shown in "Indentation Rules of Thumb" errors in orthogonal alignment can lead to larger errors than expected due to finite lateral stiffness in transducer design [1]. High lateral stiffness is a critical design element of the NMAT and is accomplished by the doubly secured indentation shaft that prevents lateral deflection when indenting and scratching samples with surface roughness or misalignment.

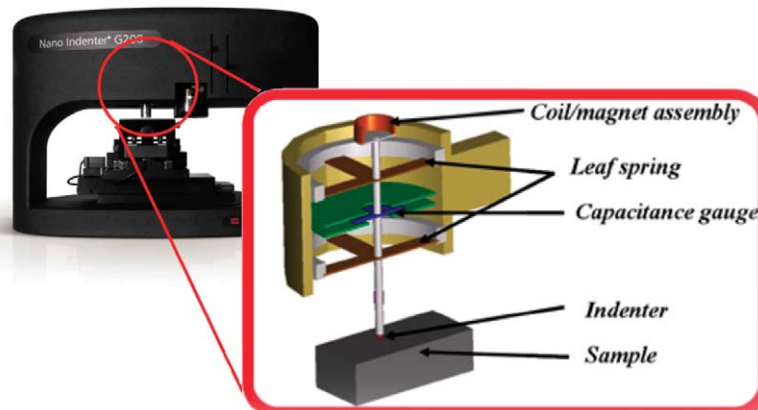


Figure 1. The Agilent Nano Indenter G200 and a cross-sectional diagram of the XP-NMAT.

Range of indenter travel	>1.5 mm
Displacement resolution	0.01 nm
Typical leaf spring stiffness	100 N/m
Maximum Load	500 mN
Load resolution	50 nN
Thermal drift rate*	0.05 nm/s

*Thermal drift rates are dependent on lab environments.

Table 2. XP-NMAT Specifications.

The final critical design component of the NMAT is the capacitance gauge which is used for sensing displacement. All commercially available nanoindenter platforms use capacitance gauges for measuring displacement. However, the capacitance gauge used in the Agilent transducers are specifically designed to allow ultra-high resolution with unparalleled displacement ranges providing users with maximum testing flexibility. Table 2 lists the specifications of the XP Nano Mechanical Actuating Transducer.

Test Procedure

Indentation Tests

To ensure measurements of mechanical properties with the highest integrity, indirect verification of the performance of the Nano Indenter G200 was completed just prior to testing the polymer samples using methods prescribed by ISO 14577, the international standard that governs hardness and mechanical properties measurements by instrumented indentation [2]. In completing this verification, two reference materials,

Corning 7980 (SiO₂) and Corning 7740 (Pyrex®) were tested at a range of forces from 10 mN to 500 mN. The results from the test method provide a Pass or Fail indication of performance for the instrument. The Pass or Fail criteria are determined by comparing the nominal values of elastic modulus supplied with the reference materials to the measured results and ensuring that the uncertainties in the measured hardness and elastic modulus are less than five percent.

To examine the full load range and the large displacement capabilities of the Nano Indenter G200, nanoindentation tests were performed on samples A, B, and C using a standard tip that allows up to 30 μm of penetration depth. The combination of the large force range and the large displacement range, without compromising instrument resolutions, allowed the complete film response to be measured. While these tests could also be performed using the ISO test method, a cyclic test method was used to highlight the repeatability of the measurements. In this test method the indenter is successively loaded multiple times up to the maximum load, in the same test location, without coming out of contact with the sample. A loading time of 3 seconds was used, with a holding time of 5 seconds and an unloading time of 3 seconds. After the final loading, the load was reduced by 90% and the force was held constant for 75 seconds to determine the drift in the sample. Following the hold for thermal drift evaluation, the indenter was withdrawn completely.

The samples listed as “D” samples were tested at elevated temperature over the range from room temperature to 100 degrees Celsius using the Hot Stage option that is available with the Nano Indenter G200. These tests used a loading time of 1.5 seconds, a hold time of 1.5 seconds, and an unloading time of 1.5 seconds. The tests performed on the hot stage were conducted quickly to avoid problems associated with thermal drift of the sample. Surface temperature of the sample was maintained at the set temperature within ± 0.1 degrees Celsius. The Hot Stage option allows elevated temperature testing to be completed using nanoindentation over the temperature range from room temperature to 350°C. While the sample is maintained at the set point temperature, an active cooling system is used to remove waste heat from the enclosure and an argon gas supply is used to encapsulate the sample and reduce corrosion on the surface; the argon gas supply is primarily used for testing at temperatures over 200°C.

Scratch Tests

A ramp-load scratch test was used to conduct five tests on each sample. In a ramp-load scratch test, a tip is brought into contact with the sample; then, the tip is loaded at a constant loading rate while simultaneously translating the sample. Prior to and following the scratch test, a single-line-scan of the surface topography is completed for comparing the original surface to the deformation caused by the scratch test. Therefore, each scratch test consists of three steps: a single-line pre-scan of the area to be scratched, the ramp load scratch test, and a final scan to evaluate the residual deformation. Before and after each step, a pre-profile and a post-profile, usually equal to 20% of the scratch length, is performed so that the software can automatically align the data in the three steps. The original and residual single-line scans allow for the evaluation of deformation mechanisms and the quantification of deformation. The scratch process is diagramed in Figure 2.

The data from the scratch test provides a plot of the aligned displacement curves on one graph so that the deformation during and after the scratch

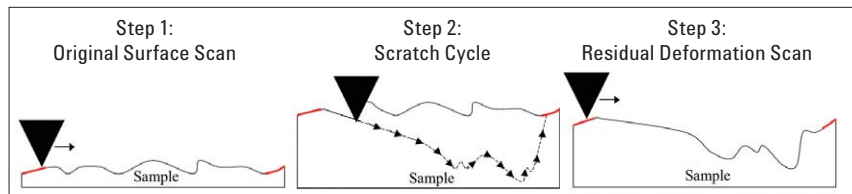


Figure 2. The three step scratch process. The red segments show the pre- and post-profiles performed during each step for aligning the data on a single graph.

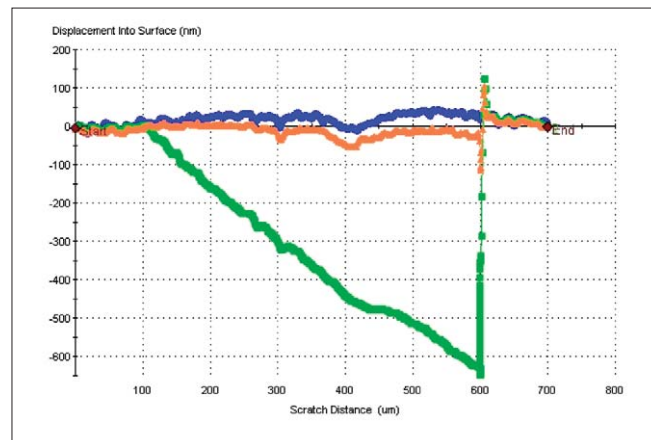


Figure 3. An example of the results from a ramp-load scratch test like the one shown in Figure 2. The original surface morphology is shown in blue, the scratch cycle is shown in green, and the residual deformation scan is shown in orange.

Samples A and B	Scratch Velocity	30 $\mu\text{m/s}$
	Ramp Load Loading Rate	1.1 mN/s
	Maximum Load	A (3 mN); B (20 mN)
Sample C	Scratch Velocity	30 $\mu\text{m/s}$
	Ramp Load Loading Rate	0.3 mN/s
	Maximum Load	C (5 mN)

Table 3. Scratch parameters for the ramp-load scratch tests. A conical tip with a 10 μm tip radius was used for testing all samples.

can easily be evaluated. Figure 3 shows an example of the aligned displacement curves from an actual scratch test. The original surface morphology is shown in blue, actual scratch cycle is shown in green, and residual deformation scan is shown in orange. In addition to the graph of the displacement curves the lateral force and critical loads are also reported as results.

When performing scratch testing on any sample set, it is critical that the test parameters of scratch velocity, loading rate, and tip geometries remain consistent throughout the samples being compared. This ensures that qualitative comparisons can be made using the resulting data. The test parameters used in testing the polymer materials are listed in Table 3. The

maximum loads vary based on the load required to induce continued failure in the samples.

The tip chosen for conducting the scratch tests was a conical tip with a radius that was approximately 10 μm . A conical tip was chosen because the films and layers were thick. Conical tips are commonly used for scratch testing when localized stress concentrations are undesirable. Another tip that is often used in scratch testing is the cube-corner tip which is a three-sided pyramid and creates a triangular projected contact with the sample; this tip geometry creates high levels of stress in the material during the scratch. Cube-corner tips are commonly used when film thicknesses are less than 2 μm .

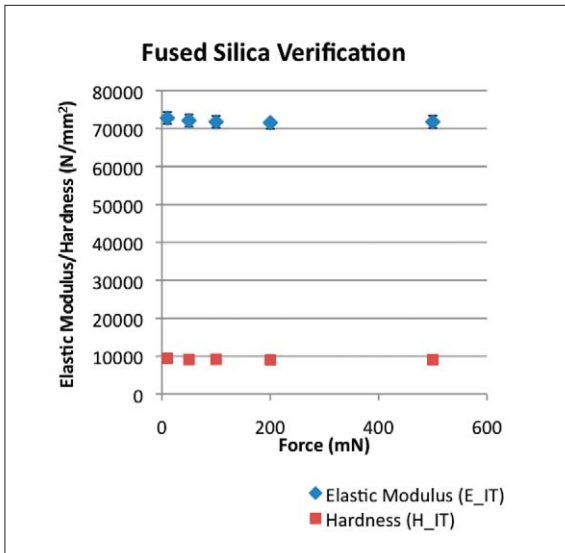


Figure 4. Results for the indirect verification of performance on the fused silica reference material.

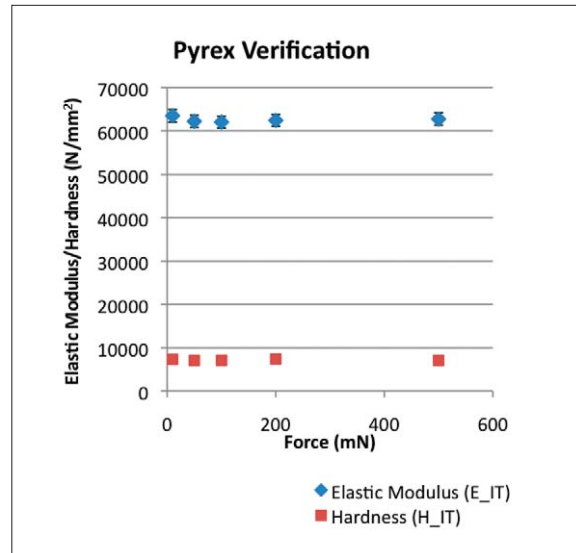


Figure 5. Results for the indirect verification of performance on the Pyrex reference material.

Results and Discussion

Indentation Test Results

Instrument Indirect Verification per ISO 14577

Fused silica and Pyrex reference materials were tested for instrument verification at loads of 500 mN, 200 mN, 100 mN, 50 mN, and 10 mN. The nominal values of the elastic modulus for the fused silica and Pyrex are 74008 N/mm² and 63256 N/mm², respectively. The results of elastic modulus and hardness on the reference materials are shown in Figure 4 and Figure 5, respectively. Each force passed verification for performance on both reference materials. In order to obtain a “Pass” for indirect verification, the instrument must measure the elastic

modulus of two materials and obtain results that are sufficiently close to the values measured by ultrasound; the algorithm for defining “sufficiently close” is prescribed in ISO 14577, Part 2, sections 5.2.5 and 5.2.6. In addition, the repeatability for hardness must be within the limit specified by the standard.

The ease of having a “Pass” or “Fail” result for the indirect verification of the instrument makes the evaluation of the instrument’s performance quick and ensures that measurements with integrity are made. As an example of the information provided for the indirect verification of the instrument, the results for the five tests completed on

the Pyrex reference material at a load of 10 mN are provided in Table 4. Notice that the second column provides a clear indication of acceptable performance.

Indentation Results for Samples A, B, and C

Samples A, B, and C were tested using standard nanoindentation with a tip that allows up to 30 μm of penetration depth. Each sample was tested over a range from 1 mN to 500 mN providing near surface results along with the bulk sample results. These samples experienced up to 11 μm of penetration depth when exposed to the maximum load of 500 mN during the tests.

Test	Verification	Maximum Force	Elastic Modulus (E_IT)	Uncertainty in E_IT (Unc. E_IT)	Hardness (H_IT)	Uncertainty in H_IT (Unc. H_IT)	Drift Correction	Test Temperature
		mN	N/mm ²	N/mm ²	N/mm ²	N/mm ²	nm/s	C
1	PASS	10	62663	1384.1	7224	158.7	-0.045	24.762
2	PASS	10	63447	1409.7	7369	163.2	-0.052	24.746
3	PASS	10	63796	1397.4	7322	161.5	-0.066	24.734
4	PASS	10	63877	1432	7281	161.5	-0.06	24.722
5	PASS	10	63629	1435.6	7282	161.3	-0.062	24.719
Mean		10	63483	1411.8	7296	161.3	-0.057	24.737
Std. Dev.		0	487	22.1	54	1.6	0.008	0.018
% COV		0.05	0.77	1.57	0.74	1	-14.81	0.07

Table 4. Results for the indirect verification at 10 mN of force on the Pyrex reference material. Notice the second column that notifies the user of a “Pass” or “Fail” for the instrument verification.

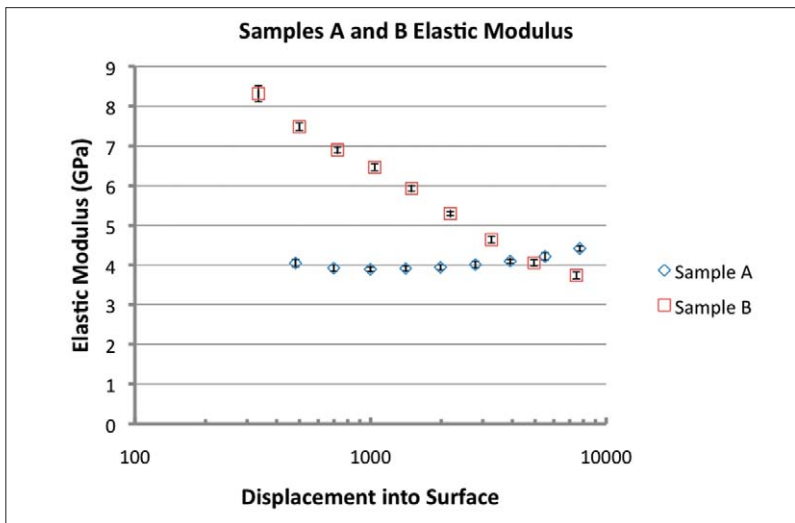


Figure 6. Elastic modulus results for samples A and B. The support of the aluminum sample puck are seen in the results for Sample A past 3000 nm of penetration.

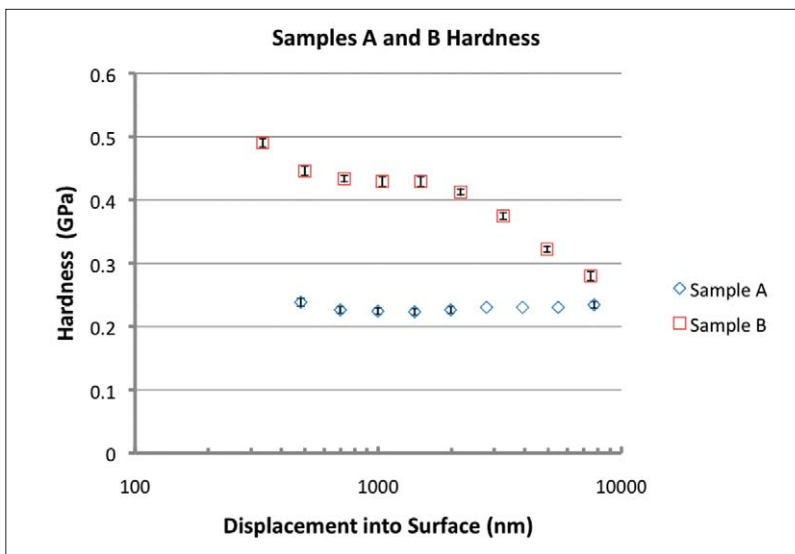


Figure 7. Hardness results for samples A and B. The coating has provided elevated hardness results to 10 μm of penetration.

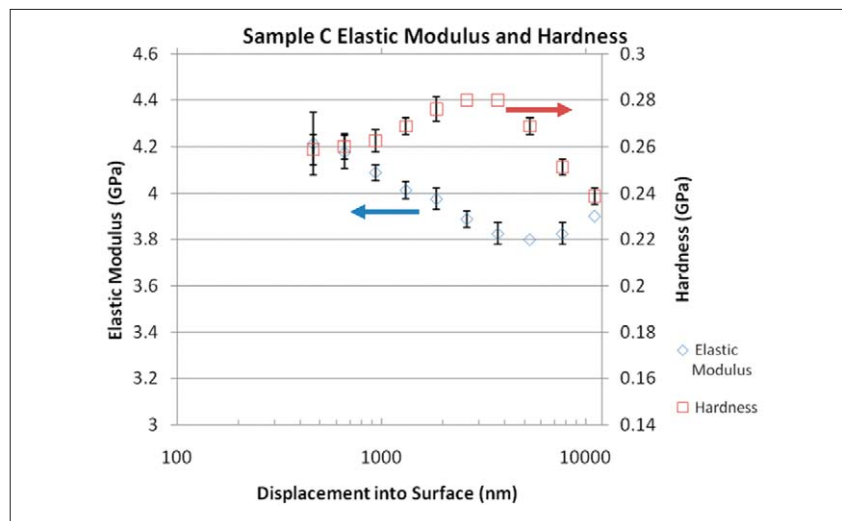


Figure 8. Elastic modulus (left axis) and hardness (right axis) results for Sample C.

The results of the elastic modulus and hardness for samples A and B are shown in Figures 6 and 7. Both of the figures show that the 13 μm hard coating on Sample B provides substantial enhancement of the mechanical properties at the surface of the sample. In Figure 6, the elastic modulus of Sample A shows a significant increase after 3 μm of penetration; however, this rise is not due to an actual change in mechanical properties, it is an artifact of having the thin sample mounted to an aluminum sample puck. Typically, hardness measurements may be made up to 10% of the films thickness, but the elastic modulus is rarely unaffected by the substrate (or in this case the mounting puck) at 10% of the film thickness. Further examination of the 10% rule-of-thumb for obtaining mechanical properties up to 10% of the film thickness is completed elsewhere [1]. Sample B does not show the effects of the sample puck because the sample is much thicker than Sample A.

Hardness results shown in Figure 7 also do not show any influence of the sample mounting puck. Hardness measurements are commonly unaffected by the underlying materials until the penetration depth becomes greater than 10% of the film thickness. The results on Sample B illustrate this response; in Figure 7 the hardness of the 13 μm coating shows properties that are unaffected by the TAC layer up to approximately 12% of the coating thickness. This coating experienced a plateau in hardness of 0.43 GPa between penetration depths of 700 nm and 1500 nm; this is a good representation of the hardness of this coating. Only a small amount of influence from the sample puck is seen in the results of hardness for Sample A and this slight influence starts appearing at 6000 nm.

Sample C also showed enhanced mechanical properties at the surface due to the 10 μm hard coating. Figure 8 displays the results for measurements of elastic modulus and hardness on Sample C. Similar to Sample B, a plateau in the hardness results are seen; however, the plateau in Sample C occurs at penetration depths that are greater than 10% of the thickness of the

coating. The results on this film show that the mechanical properties change as the film is penetrated. As opposed to a plateau in the results of elastic modulus, a minimum exists at 4000 nm of penetration. After the minimum was reached, the tests gradually reached the interface with the PMMA sheet and the elastic modulus started to increase. Undoubtedly, the hardness and elastic modulus measurements were greatly affected by the PMMA sheet at the minimums and maximums obtained from the graph in Figure 8. The reported values are probably lower than the actual values—hardness to a lesser extent—because the nominal elastic modulus for PMMA is approximately 3 GPa [3]. Since this is significantly lower than the measured values for the hard coating, the measured mechanical properties will be deflated at penetration depths that are greater than 10% of the coating thickness. The results for the elastic modulus from this sample could be more accurately determined by using a model that compensates and removes substrate influences from the results; one such model, which was developed by Rar et al., has been seamlessly integrated into the Agilent NanoSuite software to provide researchers with the ability to make substrate independent measurements of elastic modulus on films and coatings [4].

Elevated Temperature Testing of "D" Samples

The samples that were listed as "D" samples were tested at temperatures ranging from room temperature up to 100°C. Prior to elevating the temperature, each sample was tested 10 times using dynamic indentation, with the Continuous Stiffness Measurement (CSM) option, to a penetration depth of 2000 nm, to determine if the surface properties of the samples changed as a function of penetration into the sample. Figures 9 and 10 show the results for elastic modulus and hardness, respectively, for all four D samples. The benefits of the CSM option are apparent in Figures 9 and 10; this option allows the evolution of mechanical properties to be observed continuously

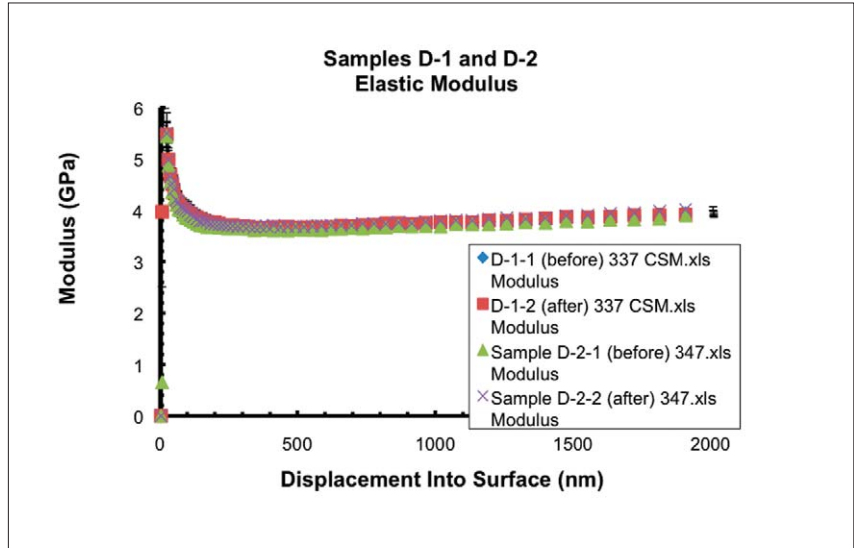


Figure 9. Elastic modulus results for the D Samples using dynamic indentation at room temperature. No separation in the mechanical response of the samples was seen as a function of penetration.

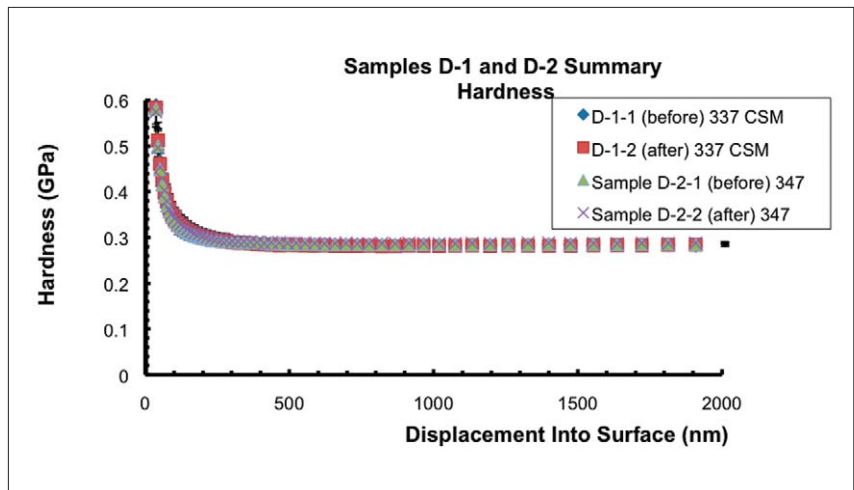


Figure 10. Hardness results for the D Samples using dynamic indentation at room temperature. No separation in the mechanical response of the samples was seen as a function of penetration.

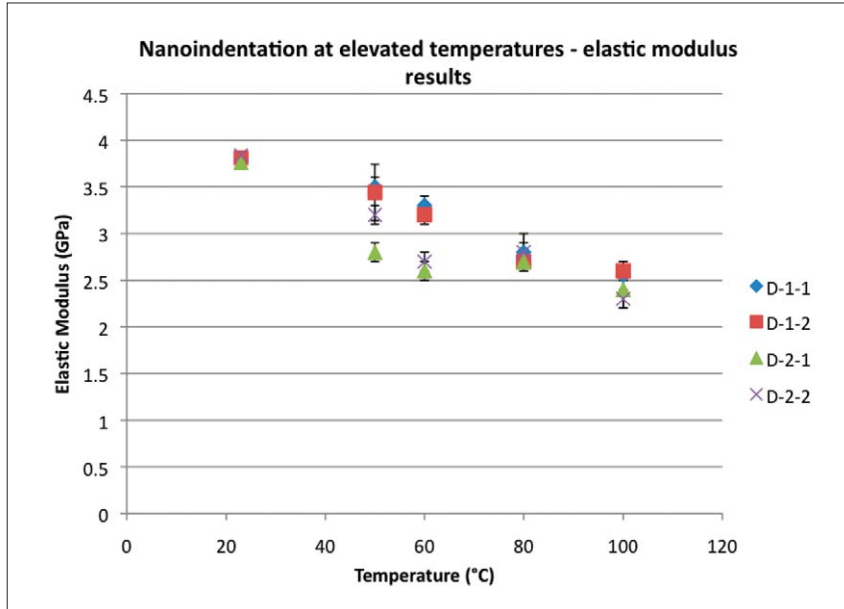


Figure 11. Elastic modulus results for the “D” samples tested at elevated temperatures.

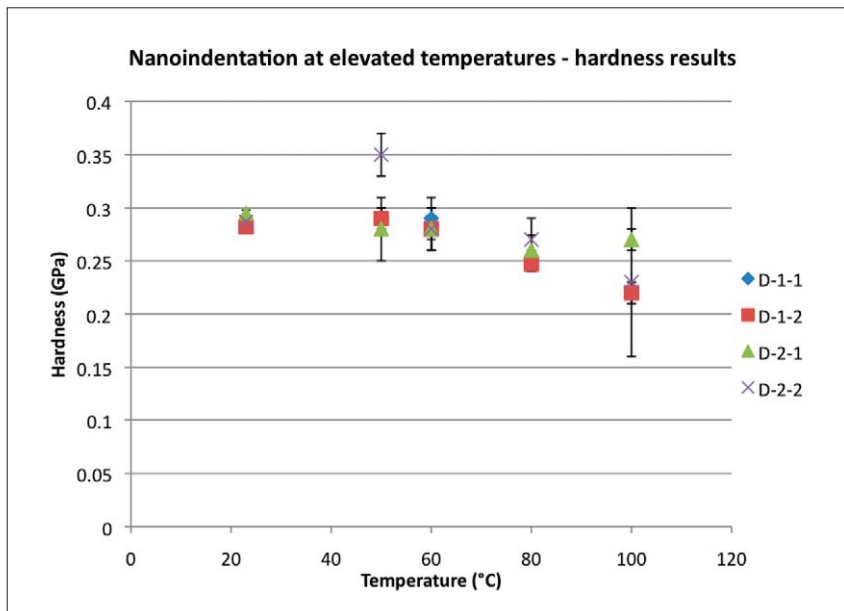


Figure 12. Hardness results for the “D” samples tested at elevated temperatures.

as a function of penetration into the surface of the sample. Surface properties just after contact along with bulk material properties can be measured with only a single indentation. Multiple indentation tests provide a measurement of repeatability for the mechanical properties of the sample; the data displayed in Figures 9 and 10 have one standard deviation errors bars displayed. This data represents the excellent repeatability of the Nano Indenter G200. It is clear from the data that, at room temperature, surface affects are not differentiators between the raw acetate propionate cellulose samples and the alcohol saponification cellulos samples.

Dynamic indentation was used at room temperature to determine if differences in surface properties were present. However, dynamic indentation is only available for room temperature testing; therefore, a set load was selected for performing quasi-static indentation tests at elevated temperatures—in application, the force limit is a user defined input and can be set to any appropriate limit. A maximum indentation load of 8 mN was selected to provide mechanical properties at approximately 1200 nm of penetration.

Ten quasi-static indentation tests to a maximum load of 8 mN were performed on each of the D samples at set temperatures of 50°C, 60°C, 80°C, and 100°C. The results, with one standard deviation error bars, of elastic modulus and hardness for the D samples are shown in Figures 11 and 12, respectively. Close examination of the results reveals that there are no major statistical differences in the mechanical properties of the raw acetate propionate cellulose samples and the alcohol saponification cellulose samples up to a temperature of 100°C. Only minor differences were observed in the measurements of elastic modulus at temperatures of 50°C and 60°C. At these temperatures the two samples listed as D-2 experienced a significant drop in elastic modulus as compared to the D-1 samples.

In Figure 12, Sample D-2-2 had an unusually high hardness at 50°C; more tests should be completed to ensure that this observed difference was not a test or positional artifact. It would be unusual for the hardness of this polymer film to increase as the temperatures increased. In addition, the results on this sample experienced a higher standard deviation as compared to the other samples tested at the same temperatures; this was especially the case for the hardness results at 100°C. The reported hardness values for Sample D-2-2 at temperatures other than 50°C were in line with the results from the other samples.

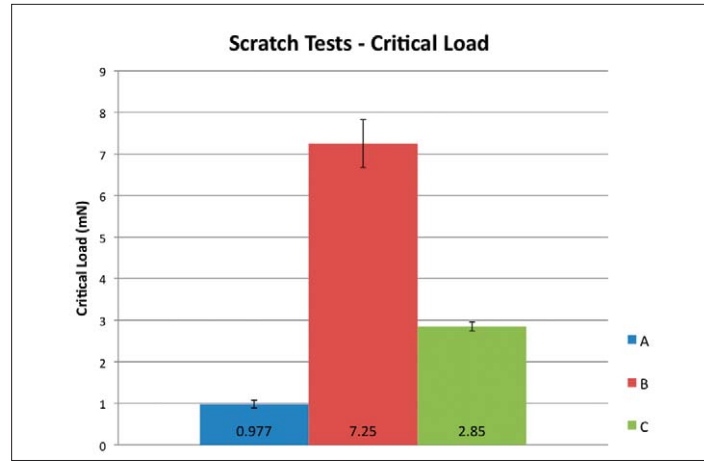


Figure 13. Results for the critical load of each sample.

Scratch Test Results

The coated samples and the bulk TAC sample were subjected to scratch testing to observe the difference in the deformation mechanisms and to evaluate failure. Each sample was scratched 8 times to ensure repeatability and establish the scatter in the results. A bar graph of the critical loads for each sample is shown in Figure 13. It is clear from the bar graph that the scratch resistance of Sample B has been greatly enhanced by its hard coating when compared to the scratch resistance of Sample A; Sample A failed at a critical load of 0.977 mN while the hard coating on Sample B failed at an average load of 7.25 mN.

Sample A

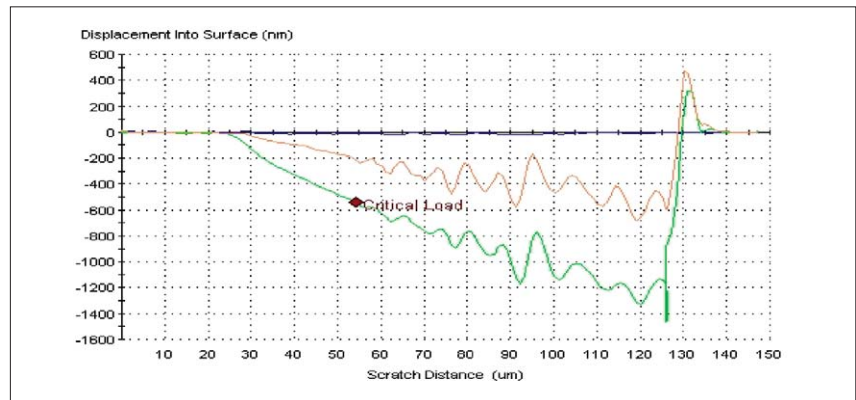


Figure 14. Scratch curves for Sample A. The blue along the x-axis is the original morphology scan, the green trace is the scratch cycle, and the orange trace is the residual deformation scan. All of the curves are aligned and shown on a common graph for the evaluation of failure and examination of deformation mechanisms.

Not only did the critical loads differ, differences in the scratch curves and the residual deformations were also apparent for each of the samples. Typical scratch curves for each of the samples tested are displayed in Figures 14 through 19; these figures show the real-time deformation of the samples as the scratch tests progressed. Along with the scratch curves for each sample, a graph of the coefficient of friction during the scratch cycle is also supplied.

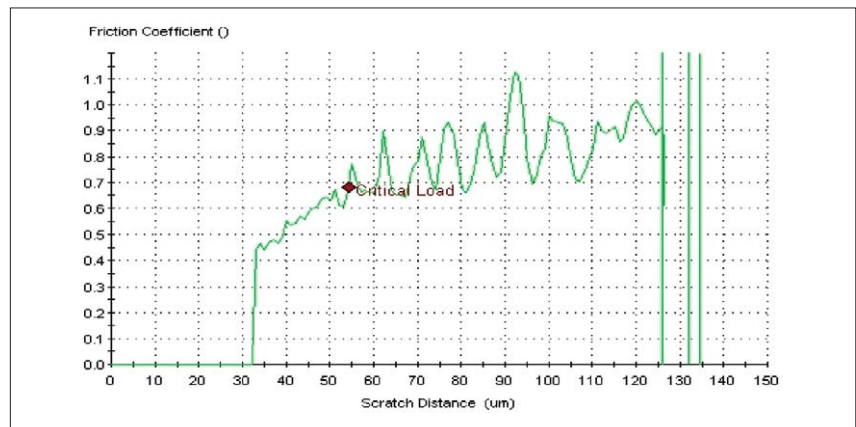


Figure 15. Coefficient of friction during the scratch cycle for Sample A. This is the coefficient of friction for the green penetration curve shown in Figure 19.

Sample B

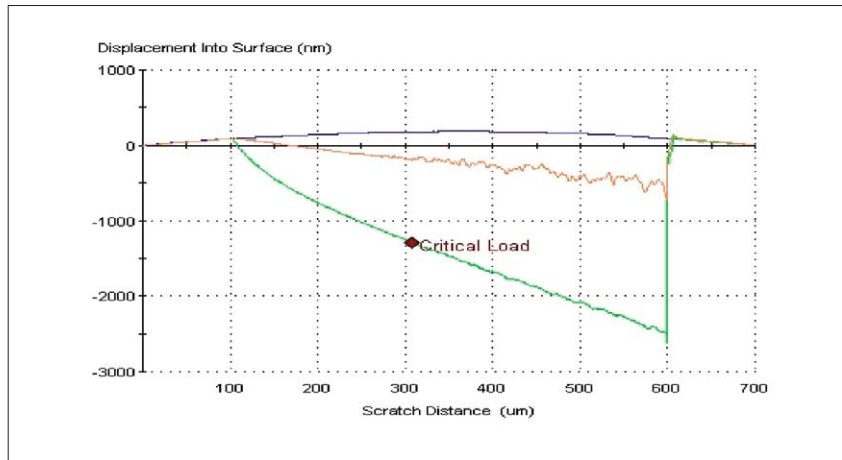


Figure 16. Scratch curves for Sample B. Notice that the scratch cycle (green curve) is smooth while the residual deformation scan (orange curve) shows fluctuation in the penetration depth. This signifies that minor fracturing is occurring instead of the ripping shown in Figure 19.

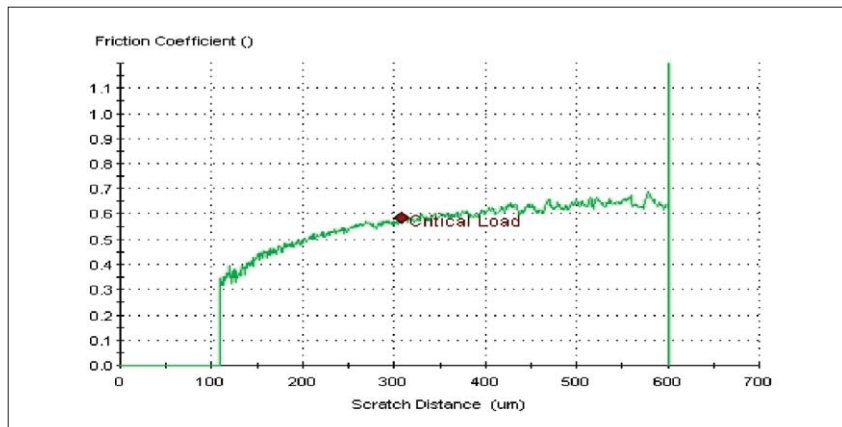


Figure 17. Coefficient of friction during the scratch cycle for Sample B. Minor fluctuations in the coefficient of friction here support the conclusion that minor fracturing is occurring during the scratch.

When comparing the scratch curves of Sample A (Figure 14) to Sample B (Figure 16), two primary differences are noticed. First, the displacement curves display dramatically different failure mechanisms. The green curve in Figure 14 (the green curve shows the path of the scratch tip during the actual scratch cycle) shows that the penetration of the scratch tip wildly fluctuates after the critical load is reached. This suggests that Sample A has experienced massive failure and the material piled up in front of the indenter and ripped off as the test progressed. Notice that the green scratch curve for Sample B does not show the wild fluctuations. During the scratch tests on Sample B, the scratch cycle progressed smoothly and the fluctuations in penetration are only seen in the orange residual deformation scan. Fluctuations in the residual deformation scan along with the absence of fluctuations in the scratch curve, as seen in the results for Sample B, are typically representative of small scale fracturing behind the scratch tip during the test—material behind the scratch tip experiences high tensile stress during the scratch cycle.

To further support the failure modes expressed in the scratch tests of Samples A and B are the differences in the graphs of the coefficient of friction during the scratch cycles. Figures 15 and 17 show the coefficient of friction for samples A and B, respectively, during the scratch cycle. The wild fluctuation in the coefficient of friction for Sample A, shown in Figure 15, make it apparent that material is being ripped off during the scratch cycle. In contrast, Sample B, shown in Figure 17, experienced a smooth slide through the sample during the scratch; very small fluctuations in the coefficient of friction are seen due to the formation of small fractures occurring behind the scratch tip.

Sample C

Similar to the scratch response of the hard coating on Sample B, Sample C smoothly deformed during the scratch cycle; the displacement curves for Sample C are shown in Figure 18 and the coefficient of friction during the scratch cycle is shown in Figure 19. Both of these figures show that small fractures occurred in the hard coating as the scratch test progressed. One of the most interesting occurrences in the failure of Sample C is shown at a scratch distance of $400\ \mu\text{m}$ in Figure 19. In this figure, the coefficient of friction experienced a step increase at the point of critical load; this step was present in all 8 tests of this sample. In addition to smooth failure, Sample C also showed a large amount of elastic recovery—the amount of elastic recovery is shown by the area bounded by the scratch cycle and the residual deformation scan (green and orange curves, respectively); permanent deformation is shown by the area bounded by the original surface scan and the residual deformation scan (blue and orange curves, respectively).

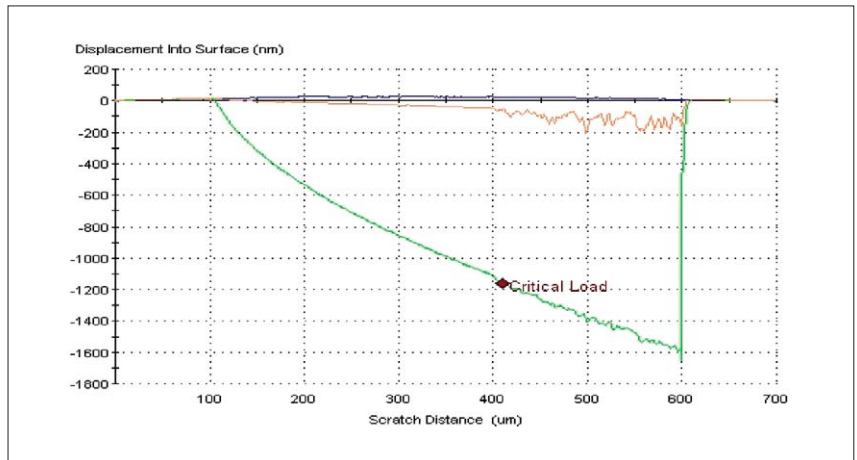


Figure 18. Scratch curves for Sample C. Just as in Sample B, smooth deformation is seen in the scratch curve (green curve) while fluctuations in the residual deformation scan (orange curve) signify minor fracturing.

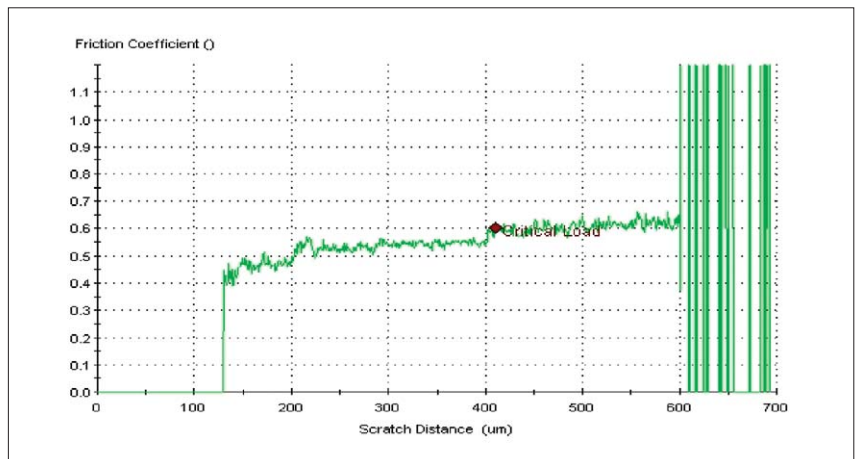


Figure 19. Coefficient of friction during the scratch cycle for Sample C. All of the tests performed on Sample C experienced a step increase in the coefficient of friction at the critical load that is located at a scratch distance of $400\ \mu\text{m}$.

Conclusions

Nanoindentation and scratch testing was completed on seven polymer samples and the results showed enhanced surface properties for the hard coated samples and excellent repeatability for all of the samples. The four "D" samples were tested using nanoindentation at elevated temperatures ranging from room temperature to 100°C. Even though two of the samples had been processed differently, the measured results of elastic modulus and hardness showed no statistical differences between the samples; this was with the exception of a minor difference seen in the results of elastic modulus at 50°C and 60°C. At these temperatures samples D-2-1 and D-2-2 experienced a statistical drop in elastic modulus as compared to samples D-1-1 and D-1-2.

The results from scratch testing showed significant differences in samples A, B, and C. the two hard coated samples experienced smooth scratching and their residual deformation scans showed minor fracturing was occurring behind the scratch tip. Sample A showed unique failure mechanisms in that during the scratch tests material was ripped off. This was clearly identifiable in the scratch curves and the residual deformation scans for this sample. Data for the coefficient of friction during the scratch cycles provided additional support for the failure mechanisms that occurred during the scratch tests.

References

1. B. Crawford. "Indentation Rules of Thumb." Agilent Technologies Application Note, 2010.
2. "Metallic Materials – Instrumented indentation test for hardness and materials parameters." ISO 14577, 2002.
3. www.efunda.com/materials/polymers/properties/polymer_datasheet.cfm?MajorID=acrylic&MinorID=4
4. A. Rar, H. Song, and G.M. Pharr. "Assessment of new relation for the elastic compliance of a film-substrate system." *Mater. Res. Soc. Symp. Proc.* 695, pp. 431–438 (2002).

Nano Mechanical Systems from Agilent Technologies

Agilent Technologies, the premier measurement company, offers high-precision, modular nano-measurement solutions for research, industry, and education. Exceptional worldwide support is provided by experienced application scientists and technical service personnel. Agilent's leading-edge R&D laboratories ensure the continued, timely introduction and optimization of innovative, easy-to-use nanomechanical system technologies.

www.agilent.com/find/nanoindenter

Americas

Canada	(877) 894 4414
Latin America	305 269 7500
United States	(800) 829 4444

Asia Pacific

Australia	1 800 629 485
China	800 810 0189
Hong Kong	800 938 693
India	1 800 112 929
Japan	0120 (421) 345
Korea	080 769 0800
Malaysia	1 800 888 848
Singapore	1 800 375 8100
Taiwan	0800 047 866
Thailand	1 800 226 008

Europe & Middle East

Austria	43 (0) 1 360 277 1571
Belgium	32 (0) 2 404 93 40
Denmark	45 70 13 15 15
Finland	358 (0) 10 855 2100
France	0825 010 700*
	*0.125 €/minute
Germany	49 (0) 7031 464 6333
Ireland	1890 924 204
Israel	972-3-9288-504/544
Italy	39 02 92 60 8484
Netherlands	31 (0) 20 547 2111
Spain	34 (91) 631 3300
Sweden	0200-88 22 55
Switzerland	0800 80 53 53
United Kingdom	44 (0) 118 9276201

Other European Countries:

www.agilent.com/find/contactus

Product specifications and descriptions in this document subject to change without notice.

© Agilent Technologies, Inc. 2010
Printed in USA, April 16, 2010
5990-5761EN



Agilent Technologies